

# Detection of $\phi \rightarrow f_0(980)\gamma$ , $\phi \rightarrow a_0(980)\gamma$ into 5 photons with KLOE at DAΦNE

The KLOE Collaboration

A. Aloisio<sup>g</sup> F. Ambrosino<sup>g</sup> A. Antonelli<sup>c</sup> M. Antonelli<sup>c</sup> C. Bacci<sup>n</sup> G. Barbiellini<sup>g</sup> F. Bellini<sup>n</sup> G. Bencivenni<sup>c</sup> S. Bertolucci<sup>c</sup> C. Bini<sup>k</sup> C. Bloise<sup>c</sup> V. Bocci<sup>k</sup> F. Bossi<sup>c</sup> P. Branchini<sup>n</sup> S. A. Bulychjov<sup>f</sup> G. Cabibbo<sup>k</sup> R. Caloi<sup>k</sup> P. Campana<sup>c</sup> G. Capon<sup>c</sup> G. Carboni<sup>m</sup> M. Casarsa<sup>g</sup> V. Casavola<sup>e</sup> G. Cataldi<sup>e</sup> F. Ceradini<sup>n</sup> F. Cervelli<sup>j</sup> F. Cevenini<sup>g</sup> G. Chiefari<sup>g</sup> P. Ciambrone<sup>c</sup> S. Conetti<sup>r</sup> E. De Lucia<sup>k</sup> G. De Robertis<sup>a</sup> P. De Simone<sup>c</sup> G. De Zorzi<sup>k</sup> S. Dell'Agnello<sup>c</sup> A. Denig<sup>c</sup> A. Di Domenico<sup>k</sup> C. Di Donato<sup>g</sup> S. Di Falco<sup>d</sup> A. Doria<sup>g</sup> M. Dreucci<sup>c</sup> O. Erriquez<sup>a</sup> A. Farilla<sup>n</sup> G. Felici<sup>c</sup> A. Ferrari<sup>n</sup> M. L. Ferrer<sup>c</sup> G. Finocchiaro<sup>c</sup> C. Forti<sup>c</sup> A. Franceschi<sup>c</sup> P. Franzini<sup>k,i</sup> C. Gatti<sup>j</sup> P. Gauzzi<sup>k</sup> A. Giannasi<sup>j</sup> S. Giovannella<sup>c</sup> E. Gorini<sup>e</sup> F. Grancagnolo<sup>e</sup> E. Graziani<sup>n</sup> S. W. Han<sup>c,b</sup> M. Incagli<sup>j</sup> L. Ingrosso<sup>c</sup> W. Kluge<sup>d</sup> C. Kuo<sup>d</sup> V. Kulikov<sup>f</sup> F. Lacava<sup>k</sup> G. Lanfranchi<sup>c</sup> J. Lee-Franzini<sup>c,o</sup> D. Leone<sup>k</sup> F. Lu<sup>c,b</sup> M. Martemianov<sup>c,f</sup> M. Matsyuk<sup>c,f</sup> W. Mei<sup>c</sup> A. Menicucci<sup>m</sup> L. Merola<sup>g</sup> R. Messi<sup>m</sup> S. Miscetti<sup>c</sup> M. Moulson<sup>c</sup> S. Müller<sup>d</sup> F. Murtas<sup>c</sup> M. Napolitano<sup>g</sup> A. Nedosekin<sup>c,f</sup> M. Palutan<sup>n</sup> L. Paoluzi<sup>m</sup> E. Pasqualucci<sup>k</sup> L. Passalacqua<sup>c</sup> A. Passeri<sup>n</sup> V. Patera<sup>l,c</sup> E. Petrolo<sup>k</sup> D. Picca<sup>k</sup> G. Pirozzi<sup>g</sup> L. Pontecorvo<sup>k</sup> M. Primavera<sup>e</sup> F. Ruggieri<sup>a</sup> P. Santangelo<sup>c</sup> E. Santovetti<sup>m</sup> G. Saracino<sup>g</sup> R. D. Schamberger<sup>o</sup> B. Sciascia<sup>k</sup> A. Sciubba<sup>l,c</sup> F. Scuri<sup>g</sup> I. Sfiligoi<sup>c</sup> J. Shan<sup>c</sup> P. Silano<sup>k</sup> T. Spadaro<sup>k</sup> E. Spiriti<sup>n</sup> G. L. Tong<sup>c,b</sup> L. Tortora<sup>n</sup> E. Valente<sup>k</sup> P. Valente<sup>c</sup> B. Valeriani<sup>d</sup> G. Venanzoni<sup>j</sup> S. Veneziano<sup>k</sup> A. Ventura<sup>e</sup> Y. Wu<sup>c,b</sup> G. Xu<sup>c,b</sup> G. W. Yu<sup>c,b</sup> P. F. Zema<sup>j</sup> Y. Zhou<sup>c</sup>

<sup>a</sup> Dipartimento di Fisica dell'Università e Sezione INFN, Bari, Italy.

<sup>b</sup> Permanent address: Institute of High Energy Physics of Academica Sinica, Beijing, China.

<sup>c</sup> Laboratori Nazionali di Frascati dell'INFN, Frascati, Italy.

<sup>d</sup> Institut für Experimentelle Kernphysik, Universität Karlsruhe, Germany.

<sup>e</sup> Dipartimento di Fisica dell'Università e Sezione INFN, Lecce, Italy.

<sup>f</sup> Permanent address: Institute for Theoretical and Experimental Physics, Moscow, Russia.

<sup>g</sup> Dipartimento di Scienze Fisiche dell'Università e Sezione INFN, Napoli, Italy.

<sup>i</sup> Physics Department, Columbia University, New York, USA.

<sup>j</sup> Dipartimento di Fisica dell'Università e Sezione INFN, Pisa, Italy.

<sup>k</sup> Dipartimento di Fisica dell'Università "La Sapienza" e Sezione INFN, Roma, Italy

<sup>l</sup> Dipartimento di Energetica dell'Università "La Sapienza", Roma, Italy.

<sup>m</sup> Dipartimento di Fisica dell'Università "Tor Vergata" e Sezione INFN, Roma, Italy

<sup>n</sup> Dipartimento di Fisica dell'Università "Roma Tre" e Sezione INFN, Roma, Italy

<sup>o</sup> Physics Department, State University of New York at Stony Brook, USA.

<sup>q</sup> Dipartimento di Fisica dell'Università e Sezione INFN, Trieste, Italy.

<sup>r</sup> Physics Department, University of Virginia, USA.

## Abstract

The KLOE detector at DAΦNE, the Frascati  $\phi$ -factory, has collected about  $30 \text{ pb}^{-1}$  by the end of 2000, corresponding to about 90 millions of  $\phi(1020)$  mesons produced. The five photon final state has been exploited to study the rare decays of  $\phi$  into  $f_0(980)\gamma$  and  $a_0(980)\gamma$ , with statistical accuracy never reached before. The preliminary results for these branching ratios, from a data sample of  $17 \text{ pb}^{-1}$ ,

are the following:  $\text{Br}(\phi \rightarrow f_0(980)\gamma) = (23.7 \pm 0.6_{stat}) \times 10^{-5}$ ,  $\text{Br}(\phi \rightarrow a_0(980)\gamma) = (5.8 \pm 0.5_{stat}) \times 10^{-5}$ . The systematic error is expected to be less than 10%, a precise evaluation is going on. For the ratio of the branching ratios of  $\phi \rightarrow f_0\gamma$  to  $\phi \rightarrow a_0\gamma$  we find  $4.1 \pm 0.4_{stat}$ .

## 1 Introduction

In the last years there has been a revival of interest in the lowest-lying scalar mesons with masses below 1 GeV which has motivated the experimental effort going on with the KLOE detector[1] at DAΦNE[2] the Frascati  $\phi$ -factory, where these resonances can be studied in detail in  $\phi$  radiative decays.

The 1 GeV region is an interesting and challenging domain: on one side it is far below the perturbative QCD regime, on the other side strict Chiral Perturbation Theory is not expected to make reliable predictions at these energy values where resonance effects can show up. This region has thus become an important test ground both for analyses based both on QCD sum-rules[3] and for effective chiral models[4, 5, 6].

The controversial nature of the  $f_0(980)$ ,  $a_0(980)$ [7] and the poor knowledge of their properties adds further interest to this 1 GeV energy region: along the years several proposals have been suggested concerning the constitution of these scalars as complex  $q\bar{q}q\bar{q}$  states[8],  $K\bar{K}$  molecules[9] or ordinary  $q\bar{q}$  mesons[10]. A precise measurement of  $\text{Br}(\phi \rightarrow f_0\gamma)$ ,  $\text{Br}(\phi \rightarrow a_0\gamma)$  and of the ratio of these branching ratios can help in better establishing the nature of these mesons[11].

In this paper we describe the preliminary results on the decays  $\phi \rightarrow f_0\gamma$ ,  $a_0\gamma \rightarrow 5\gamma$  from the analysis of  $17 \text{ pb}^{-1}$ , corresponding to about 50 millions of  $\phi$  decays, from the data sample collected by KLOE in the year 2000. A peculiar aspect of these decays is that both the branching ratio and the resonance mass shape depend strongly on the meson structure. Therefore, the analysis follows a scheme independent as much as possible on the model implemented in the Montecarlo.

## 2 Selection criteria for five photon events

The events are characterized by the presence of five prompt photons, i.e. photons coming from the interaction point (I.P.) of DAΦNE. These photons are detected as energy deposits in the calorimeter that satisfy the condition  $t - r/c = 0$ , where  $t$  is the arrival time,  $r$  is the distance of the cluster from the I.P. and  $c$  is the speed of light. We define a photon to be “prompt” if  $|t - r/c| < 5\sigma_t$ [12]. An acceptance angular region corresponding to the polar angle interval  $21^\circ - 159^\circ$  is defined for the prompt photons, in order to exclude the blind region around the beam-pipe. The processes that mainly contribute to the five photon final state are the following:

- $\phi \rightarrow f_0\gamma \rightarrow \pi^0\pi^0\gamma$
- $\phi \rightarrow \rho^0\pi^0 \rightarrow \pi^0\pi^0\gamma$
- $\phi \rightarrow a_0\gamma \rightarrow \eta\pi^0\gamma$  ( $\eta \rightarrow \gamma\gamma$ )
- $\phi \rightarrow \rho^0\pi^0 \rightarrow \eta\pi^0\gamma$  ( $\eta \rightarrow \gamma\gamma$ )

and the non resonant ones:

- $e^+e^- \rightarrow \omega\pi^0 \rightarrow \pi^0\pi^0\gamma$
- $e^+e^- \rightarrow \omega\pi^0 \rightarrow \eta\pi^0\gamma$  ( $\eta \rightarrow \gamma\gamma$ )

Also the three and seven photon final states

- $\phi \rightarrow \eta\gamma \rightarrow \gamma\gamma\gamma$

- $\phi \rightarrow \pi^0 \gamma \rightarrow \gamma \gamma \gamma$
- $e^+ e^- \rightarrow \gamma \gamma (\gamma)$
- $\phi \rightarrow \eta \gamma \rightarrow \pi^0 \pi^0 \pi^0 \gamma$

have to be taken into account, because they can simulate five photon events due to machine background and cluster splitting or merging of close photons and loss of soft photons.

The analyses described in this paper make use of a constrained fit ensuring kinematic closure of the events. The free parameters of the fit are: the three coordinates (x, y, z) of the impact point on the calorimeter, the energy and the time of flight for each photon coming from the I.P., the two energies of the beams and the three coordinates of the position of the I.P.. The analysis procedure adopted is the following:

1. fully neutral events with exactly five prompt photons are selected;
2. the kinematic fit is applied on these events a first time with the constraints of the total energy and momentum conservation and satisfying  $t - r/c = 0$  for each prompt photon;
3. the photon pairing is performed looking for the best combination, by minimizing the appropriate  $\chi^2$  for each of the following hypotheses:  $\pi^0 \pi^0 \gamma$ ,  $\eta \pi^0 \gamma$ ,  $\omega \pi^0$ ,  $\eta \gamma \rightarrow \gamma \gamma \gamma$  and  $\pi^0 \gamma$ .
4. the kinematic fit is applied again to each of the best combination constraining also the invariant masses of the photon pairs assigned to  $\pi^0$  and  $\eta$ , without any assumption on the  $f_0$  and  $a_0$  mass.

### 3 $\phi \rightarrow \pi^0 \pi^0 \gamma$

The main background channels, with the expected signal to background (S/B) ratio obtained from [13, 14, 15, 16], are listed in Tab. 1. After applying the first kinematic fit, the best photon combination producing the two  $\gamma \gamma$  pairs with  $\pi^0$  mass is searched for with the additional condition  $M_{\pi\pi} > 700$  MeV (the expected  $f_0$  mass region). According to our simulation, this procedure correctly assigns photons in 95% of the cases. The analysis cuts to select  $\phi \rightarrow f_0 \gamma \rightarrow \pi^0 \pi^0 \gamma$  events are:

1.  $\chi_{\pi\pi\gamma}^2/\text{ndf} < 5$ ;
2.  $5\sigma$  cut on the reconstructed  $\pi^0$ 's mass (the output of the first kinematic fit, without mass constraints, is used);
3.  $\cos \psi_{\omega\pi} > 0.4$ , where  $\psi$  is the angle between the primary photon and the pion's flight direction in the  $\pi^0 \pi^0$  rest frame. This cut is performed to reduce the  $\phi \rightarrow a_0 \gamma$  and  $\phi \rightarrow \rho^0 \pi^0$  backgrounds;
4.  $\chi_{\omega\pi}^2/\text{ndf} < 3$  and a  $3\sigma$  cut on the reconstructed  $\omega$  mass to veto  $e^+ e^- \rightarrow \omega \pi^0$ ;
5.  $E_{\text{tot}} > 900$  MeV and  $175^\circ < \Delta\phi < 185^\circ$  for the two most energetic photons to reject  $e^+ e^- \rightarrow \gamma \gamma (\gamma)$ ;
6.  $3\sigma$  cut on the radiative photon energy ( $E_{\gamma \text{ rad}} \sim 500$  MeV) to reject  $\phi \rightarrow \pi^0 \gamma$ .

In order to evaluate the analysis efficiency as a function of  $M_{\pi\pi}$ , the generated  $f_0$  mass has been divided into 20 MeV bins. The total variation of the efficiency does not exceed 30% of the mean value, which is reported in tab. 1 together with the efficiencies for the background channels.

A fit procedure is in progress to evaluate the branching ratio and to obtain the  $f_0$  mass shape by folding the available theoretical  $dN/dM$  shapes with the reconstruction effects. Since this procedure is not completed and a reasonable  $f_0$  mass shape was chosen in the Montecarlo, the branching ratio is evaluated using bin by bin efficiency while data and Montecarlo distributions are compared as follows:

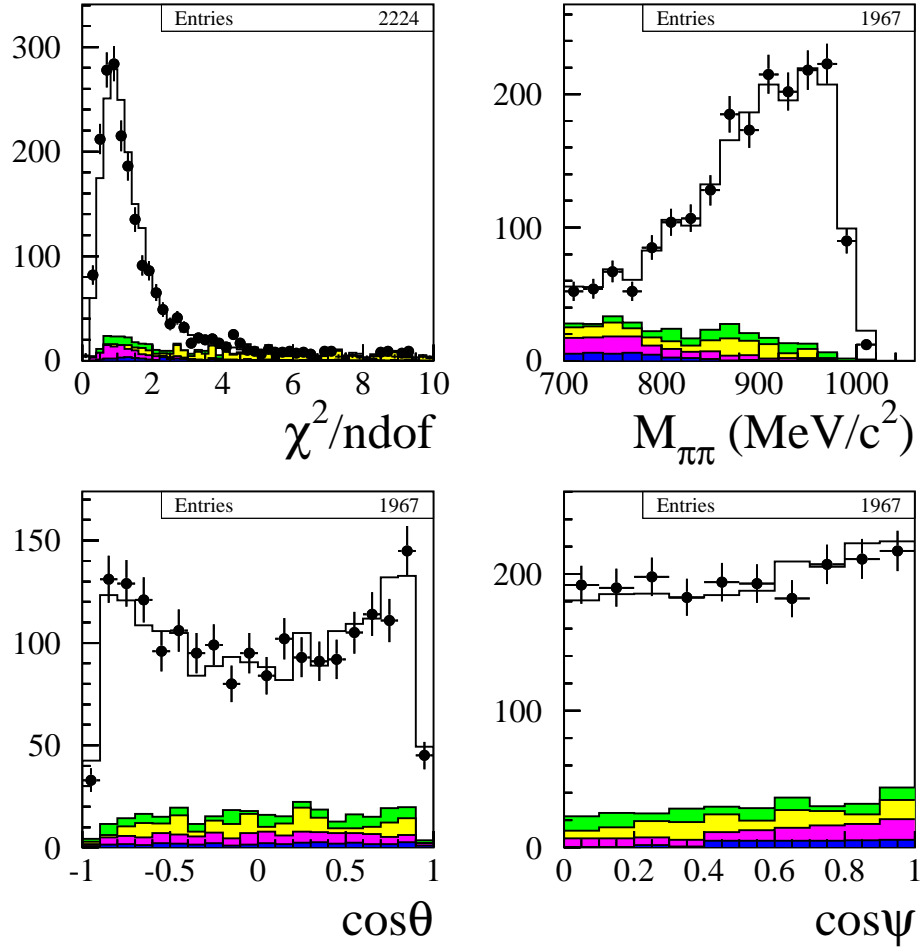


Figure 1:  $\phi \rightarrow f_0 \gamma \rightarrow \pi^0 \pi^0 \gamma$  distributions:  $\chi^2/\text{ndf}$  (up-left),  $\pi^0 \pi^0$  invariant mass (up-right), polar angle (down-left) and  $\cos \psi$  (down-right). Black circles are data, solid histograms are the expected MC signal+background spectra while the background contributions are displayed in colors: green is  $e^+ e^- \rightarrow \omega \pi^0$ , yellow is  $\phi \rightarrow \eta \gamma$ , magenta is  $\phi \rightarrow \rho \pi^0$  and blue is  $\phi \rightarrow a_0 \gamma$ . The MC  $f_0$  shapes have been obtained by weighting the  $M_{\pi\pi}$  bin contents to reproduce the shape of the data.

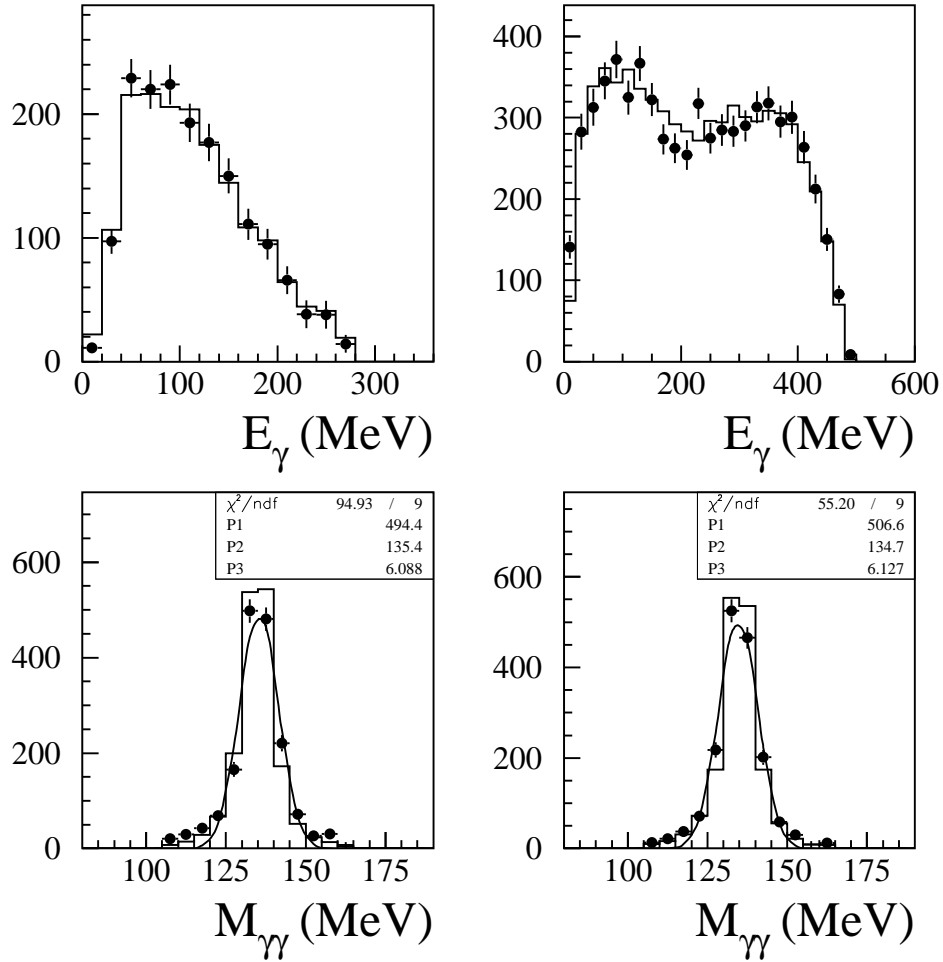


Figure 2:  $\phi \rightarrow f_0 \gamma \rightarrow \pi^0 \pi^0 \gamma$  events: energy distributions (up) [left: radiative photon, right:  $\gamma$ 's from pions] and the two  $\pi^0$  masses (down). Black circles are data after background subtraction, solid histograms are the expected spectra for the signal. The MC  $f_0$  shapes have been obtained by weighting the  $M_{\pi\pi}$  bin contents to reproduce the shape of the data.

| Decay channel  | Natural S/B | Analysis efficiency |
|--|-------------|---------------------|
| $\phi \rightarrow f_0\gamma \rightarrow \pi^0\pi^0\gamma$                                    | —           | 39.7%               |
| $e^+e^- \rightarrow \omega\pi^0 \rightarrow \pi^0\pi^0\gamma$                                | 0.6         | 1.2%                |
| $\phi \rightarrow \rho^0\pi^0 \rightarrow \pi^0\pi^0\gamma$                                  | 3.7         | 4.9%                |
| $\phi \rightarrow a_0\gamma \rightarrow \eta\pi^0\gamma \rightarrow \gamma\gamma\pi^0\gamma$ | 3.5         | 1.9%                |
| $\phi \rightarrow \eta\gamma \rightarrow \pi^0\pi^0\pi^0\gamma$                              | 0.02        | $5 \times 10^{-4}$  |

Table 1: S/B ratios and analysis efficiencies for the  $\phi \rightarrow f_0\gamma \rightarrow \pi^0\pi^0\gamma$  decay and related background.

1.  $\phi \rightarrow f_0\gamma$  MC events are analyzed in slices of  $M_{\pi\pi}$  to obtain the various histograms shapes;
2. after subtracting the expected background from the observed  $M_{\pi\pi}$  distribution, for each  $M_{\pi\pi}$  bin we evaluate the scale factor that, applied on the MC  $M_{\pi\pi}$  shape, reproduces data;
3. these scale factors are then applied to all MC “sliced” histograms which are then summed to produce the MC distributions to be compared with the data.

This implies that any effect of bad event reconstruction that gives rise to a distorted  $M_{\pi\pi}$  shape is neglected. We expect such contribution mainly from bad photons’ reconstruction ( $\sim 4 \div 5\%$ ) and wrong  $\gamma$ ’s pairing. The data–Montecarlo comparison for the most relevant distributions after this procedure is shown in Fig. 1. The behaviour of the energy spectra and of the pion masses after the background subtraction is also reported (Fig. 2).

Applying the analysis to the  $17 \text{ pb}^{-1}$ , 1967 events survive while the Montecarlo expected background contribution is  $305 \pm 13_{\text{stat}}$ . The corresponding branching ratio has been evaluated by normalization with respect to the  $\phi \rightarrow \eta\gamma \rightarrow \gamma\gamma\gamma$  events, using the PDG[16] value for the  $\text{Br}(\phi \rightarrow \eta\gamma \rightarrow \gamma\gamma\gamma)$ . Neglecting the interference between the signal and  $\phi \rightarrow \rho\pi^0 \rightarrow \pi^0\pi^0\gamma$ , the final branching ratio is:

$$\text{Br}(\phi \rightarrow f_0\gamma \rightarrow \pi^0\pi^0\gamma) = (7.9 \pm 0.2_{\text{stat}}) \times 10^{-5}. \quad (1)$$

for  $M_{\pi\pi} > 700 \text{ MeV}$ .

The systematic error is under study and it should not exceed 10%.

## 4 $\phi \rightarrow \eta\pi^0\gamma$

The  $\phi \rightarrow \eta\pi^0\gamma$  events, with  $\eta \rightarrow \gamma\gamma$ , have been considered to study the  $\phi \rightarrow a_0\gamma$  decay. The corresponding S/B ratio of the signal and the main background channels are reported in tab.2.

A first selection to reject  $e^+e^- \rightarrow \gamma\gamma(\gamma)$  events has been applied. Then the  $\eta\gamma \rightarrow \gamma\gamma\gamma$  contamination is eliminated by rejecting events with a two photon invariant mass near the  $\eta$  mass together with another photon energy near 363 MeV.

In order to reduce the  $\pi^0\pi^0\gamma$  background, the photon combination obtained for the  $e^+e^- \rightarrow \omega\pi^0 \rightarrow \pi^0\pi^0\gamma$  hypothesis has been exploited. The correlation between the angle  $\psi$  (angle between the non associated photon and the primary  $\pi^0$  in the dipion rest frame), and the energy of the non associated photon is shown in fig.3.a,b for MC samples and in fig.3.c for data. From the comparison several contributions can be identified. In order to avoid introducing any bias in the unknown  $a_0$  shape, the analysis cuts have been studied using a  $\phi \rightarrow \eta\pi^0\gamma$  MC sample with an almost flat  $\eta\pi^0$  invariant mass. That sample is compared in fig.3.d with the dominant background; also the applied cut is shown.

Since the  $\phi \rightarrow \rho^0\pi^0 \rightarrow \pi^0\pi^0\gamma$  events populate the same region of the scatter plot of fig.3 as the signal, this contamination should be reduced by using different variables. The choosen ones are shown in the scatter plot of fig.4: the difference between the  $\chi^2$  of the second fit in the hypotheses  $\pi^0\pi^0\gamma$  and  $\eta\pi^0\gamma$

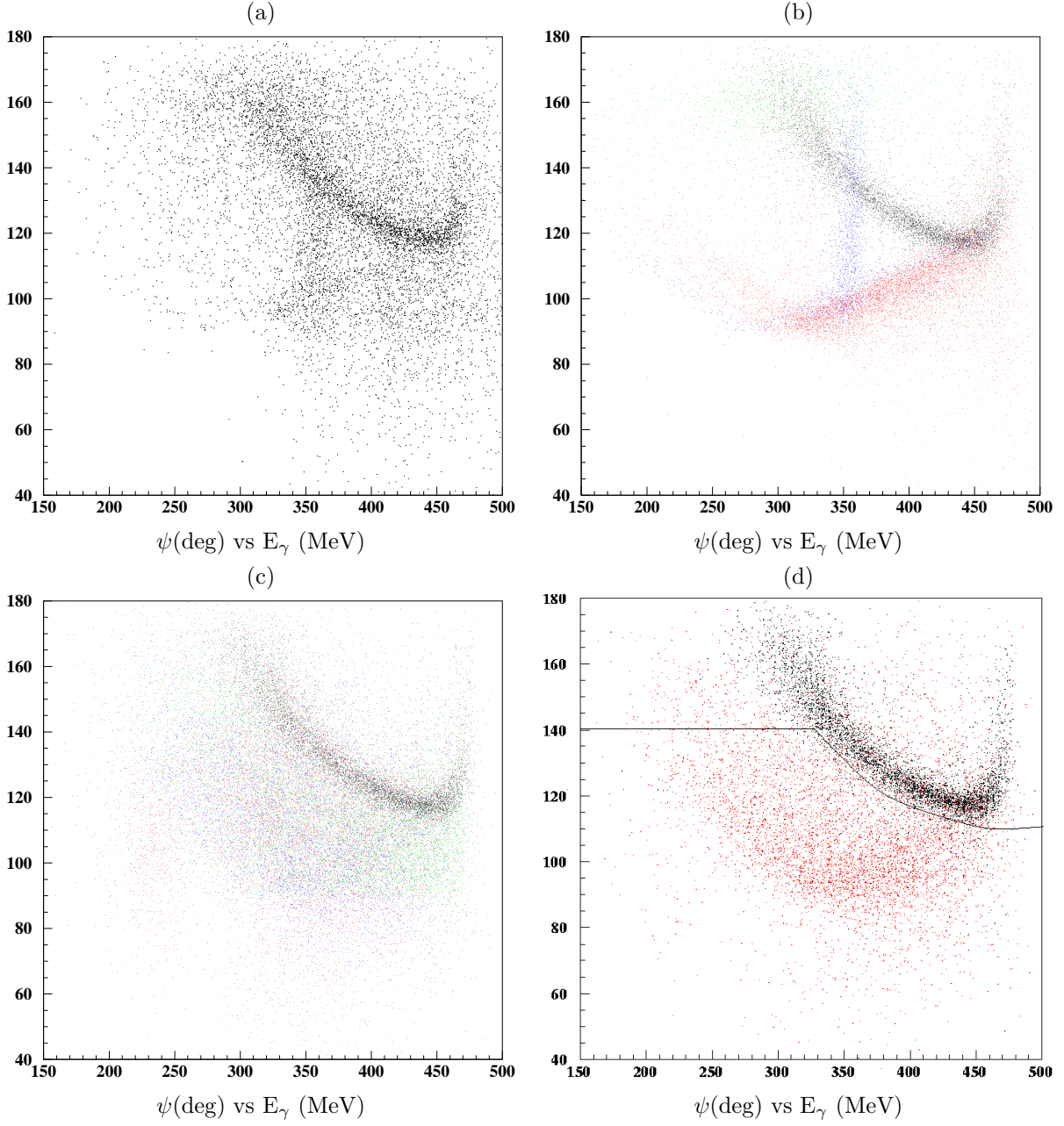


Figure 3:  $\psi$  vs  $E_\gamma$  - (a) Data; (b) MC: black -  $\omega\pi^0 \rightarrow \pi^0\pi^0\gamma$ , red -  $a_0\gamma \rightarrow \eta\pi^0\gamma$ , green -  $f_0\gamma \rightarrow \pi^0\pi^0\gamma$ , blue -  $\eta\gamma \rightarrow \gamma\gamma\gamma$ ; (c) MC: black -  $\omega\pi^0 \rightarrow \pi^0\pi^0\gamma$ , red -  $\rho^0\pi^0 \rightarrow \pi^0\pi^0\gamma$ , green -  $\rho^0\pi^0 \rightarrow \eta\pi^0\gamma$ , blue -  $\omega\pi^0 \rightarrow \eta\pi^0\gamma$ ; (d) MC: black -  $\omega\pi^0 \rightarrow \pi^0\pi^0\gamma$ ; red -  $\eta\pi^0\gamma$  flat (see text); the accepted region is below the solid line.

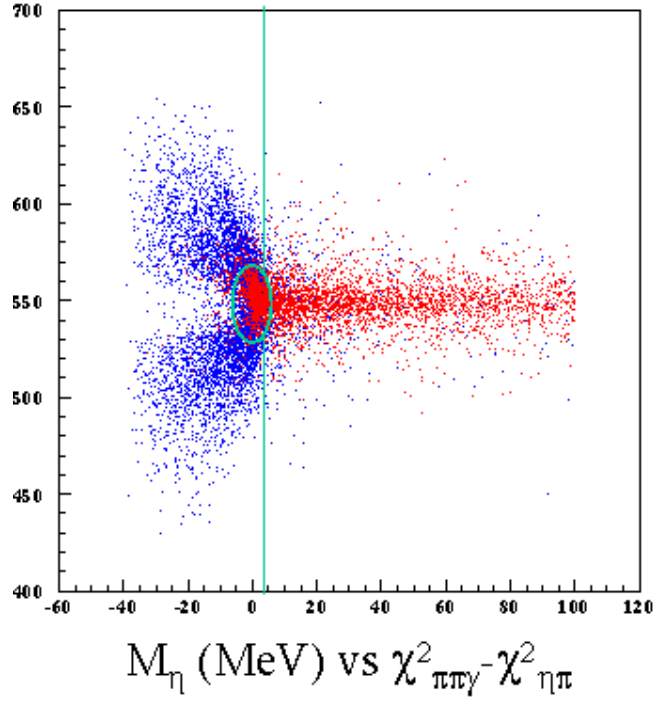


Figure 4:  $\eta$  reconstructed mass vs  $\chi^2_{\pi\pi\gamma} - \chi^2_{\eta\pi}$  for MC samples: red -  $\eta\pi^0\gamma$  flat; blue -  $\rho^0\pi^0 \rightarrow \pi^0\pi^0\gamma$ ; the applied cut is also shown.

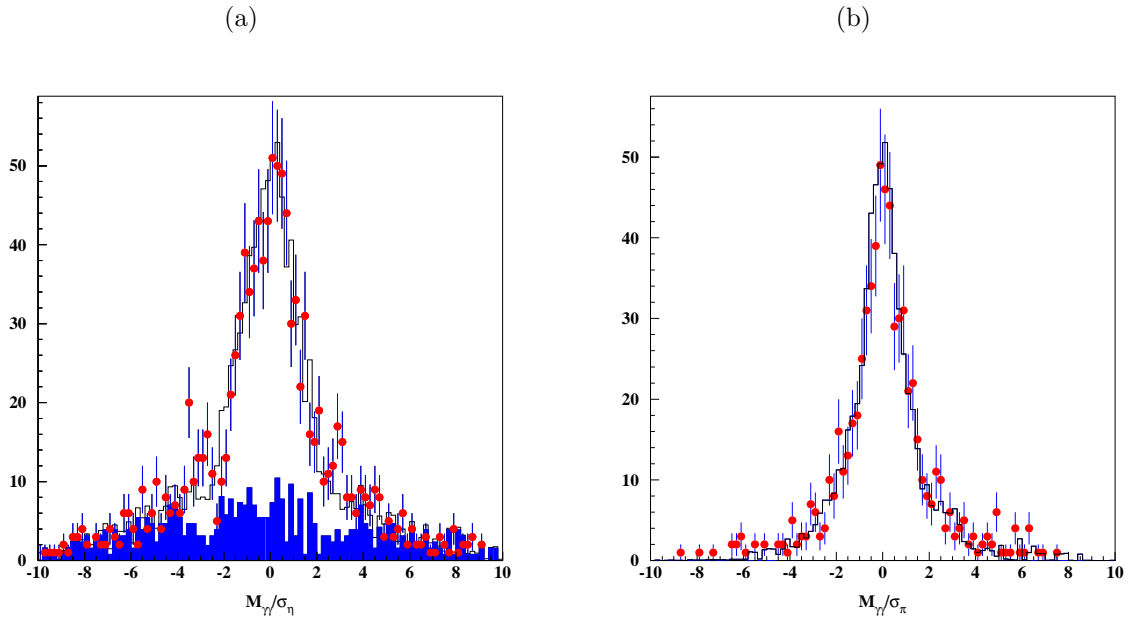


Figure 5: (a) Reconstructed  $\eta$  mass divided by the resolution; full histogram:  $\eta\gamma \rightarrow \pi^0\pi^0\pi^0\gamma$  (MC); (b) Reconstructed  $\pi^0$  mass divided by the resolution.

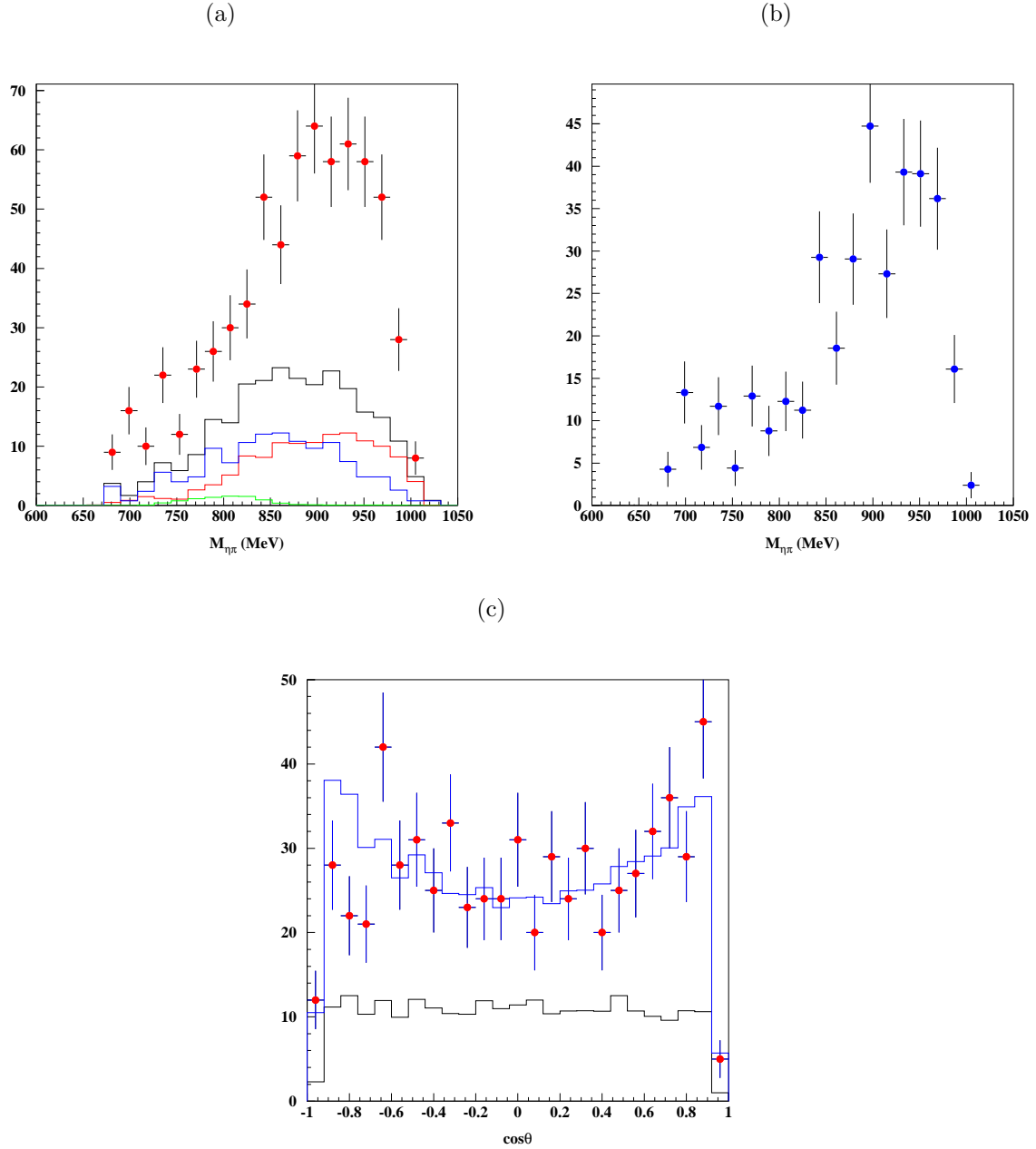


Figure 6: (a)  $\eta\pi^0$  invariant mass - points: data, histograms: background spectra (MC), red -  $\pi^0\pi^0\gamma$ , green -  $e^+e^- \rightarrow \omega\pi^0 \rightarrow \eta\pi^0\gamma$ , blue -  $\eta\gamma \rightarrow \pi^0\pi^0\pi^0\gamma$ , black - total; (b)  $\eta\pi^0$  invariant mass background subtracted; (c)  $\cos\vartheta$  distribution - points: data, histograms: background, signal plus background.

| Process   | Natural S/B          | Final efficiency            |
|---|----------------------|-----------------------------|
| $\phi \rightarrow a_0\gamma \rightarrow \eta\pi^0\gamma$        | –                    | 27.2%                       |
| $\phi \rightarrow \rho^0\pi^0 \rightarrow \eta\pi^0\gamma$      | 5.3                  | 27.1%                       |
| $e^+e^- \rightarrow \omega\pi^0 \rightarrow \eta\pi^0\gamma$    | 71                   | 25.8%                       |
| $e^+e^- \rightarrow \omega\pi^0 \rightarrow \pi^0\pi^0\gamma$   | 0.14                 | $3.5 \times 10^{-3}$        |
| $\phi \rightarrow \rho^0\pi^0 \rightarrow \pi^0\pi^0\gamma$     | 1                    | 5.0%                        |
| $\phi \rightarrow f_0\gamma \rightarrow \pi^0\pi^0\gamma$       | 0.27                 | $1.4-3.0 \times 10^{-3(*)}$ |
| $\phi \rightarrow \eta\gamma \rightarrow \gamma\gamma\gamma$    | $6.1 \times 10^{-3}$ | $3.3 \times 10^{-6}$        |
| $\phi \rightarrow \eta\gamma \rightarrow \pi^0\pi^0\pi^0\gamma$ | $7.5 \times 10^{-3}$ | $5.4 \times 10^{-4}$        |

Table 2: S/B ratios and efficiencies for  $\eta\pi^0\gamma$  decay and related background.

(\*)Depending on the  $f_0$  shape.

and the reconstructed  $\eta$  mass. The accepted region is defined by  $\chi^2_{\pi^0\pi^0\gamma} - \chi^2_{\eta\pi^0\gamma} > 3$  plus the internal part of the ellipse.

Last contamination that has to be reduced is  $\phi \rightarrow \eta\gamma \rightarrow \pi^0\pi^0\pi^0\gamma$ . In fig.5.a is reported the invariant mass of the two photons associated to the  $\eta$ ; the comparison with the MC shows that the background events mainly populate the tails of the distribution. A two standard deviation cut is then applied to reduce the  $\eta\gamma$  contamination. The final efficiencies are reported in tab.2.

At the end of the selection procedure 666 events survive. The expected number of background events is  $253 \pm 11$  mainly due to  $\phi \rightarrow \rho^0\pi^0 \rightarrow \pi^0\pi^0\gamma$  and  $\phi \rightarrow \eta\gamma \rightarrow \pi^0\pi^0\pi^0\gamma$ . The invariant mass of  $\eta\pi^0$  is shown in fig.6, together with the  $\cos\theta$  distribution for the non associated photon. The corresponding branching ratio is:

$$Br(\phi \rightarrow \eta\pi^0\gamma) = (7.4 \pm 0.5_{stat}) \times 10^{-5} \quad (2)$$

The systematic error is still under study; according to preliminary evaluations it should not exceed 10%. This result is in agreement, within the errors, with the values published by the VEPP-2M experiments[14, 17] and with the KLOE result of the analysis of the 1999 statistics[18].

The branching ratio (2) includes the  $\phi \rightarrow \rho^0\pi^0 \rightarrow \eta\pi^0\gamma$  contribution. If the interference of this process with  $\phi \rightarrow a_0\gamma \rightarrow \eta\pi^0\gamma$  is negligible[19], one can subtract the  $\rho^0\pi^0$  contribution. To evaluate the number of expected  $\rho^0\pi^0$  events, the average of the very recent measurements of the  $Br(\rho^0 \rightarrow \eta\gamma)$  performed by the two VEPP-2M experiments[20] has been used. This average value turns out to be  $Br(\rho^0 \rightarrow \eta\gamma) = (3.0 \pm 0.3) \times 10^{-4}$  (which is different from the PDG value[16]  $Br(\rho^0 \rightarrow \eta\gamma) = (2.4 \pm 0.9) \times 10^{-4}$ ), from which follows an expected number of  $86 \pm 9$   $\rho^0\pi^0 \rightarrow \eta\pi^0\gamma$  events. After the subtraction one obtains:

$$Br(\phi \rightarrow a_0\gamma \rightarrow \eta\pi^0\gamma) = (5.8 \pm 0.5_{stat}) \times 10^{-5} \quad (3)$$

## 5 $\phi \rightarrow f_0\gamma$ to $\phi \rightarrow a_0\gamma$ ratio

From the results described in the previous sections a preliminary estimate of the ratio of the two branching ratios can be obtained. Assuming that  $\pi^0\pi^0\gamma$  and  $\eta\pi^0\gamma$  are the dominant decay modes of respectively  $f_0$  and  $a_0$  and using the values of eqs.(1) and (3), one obtains (with  $Br(\phi \rightarrow f_0\gamma) = 3Br(\phi \rightarrow f_0\gamma \rightarrow \pi^0\pi^0\gamma)$ ):

$$\frac{Br(\phi \rightarrow f_0\gamma)}{Br(\phi \rightarrow a_0\gamma)} = 4.1 \pm 0.4_{stat} \quad (4)$$

in reasonable agreement with the prediction given in [11].

## 6 Conclusions

Events with five prompt photon have been selected from a sample of  $17 \text{ pb}^{-1}$  of the data collected by KLOE in 2000, corresponding to about 50 millions of  $\phi$  meson produced. From the analysis of the  $\pi^0\pi^0\gamma$  channel, a  $\text{Br}(\phi \rightarrow f_0(980)\gamma \rightarrow \pi^0\pi^0\gamma) = (7.9 \pm 0.2_{stat}) \times 10^{-5}$  has been obtained. The result of the analysis of the  $\eta\pi^0\gamma$  with  $\eta \rightarrow \gamma\gamma$  channel, is:  $\text{Br}(\phi \rightarrow \eta\pi^0\gamma) = (7.4 \pm 0.5_{stat}) \times 10^{-5}$ . By subtracting the expected  $\phi \rightarrow \rho^0\pi^0 \rightarrow \eta\pi^0\gamma$  contribution, one can evaluate  $\text{Br}(\phi \rightarrow a_0(980)\gamma \rightarrow \eta\pi^0\gamma) = (5.8 \pm 0.5_{stat}) \times 10^{-5}$ . The ratio of the branching ratio  $\phi \rightarrow f_0\gamma$  to  $\phi \rightarrow a_0\gamma = 4.1 \pm 0.4_{stat}$  is obtained.

Work is in progress to fit the spectra and to extract the  $f_0$  and  $a_0$  resonance parameters.

## References

- [1] KLOE Collaboration, KLOE: a general purpose detector for DAΦNE, LNF-92/019 (IR) (1992); KLOE Collaboration, The KLOE detector - Technical Proposal, LNF-93/002 (IR) (1993).
- [2] S. Guiducci et al., Proceedings of PAC99, New York, March 1999.
- [3] F. De Fazio and M. Pennington, hep-ph/0104289, June 2001.
- [4] E. Oset et al., Physics and detectors for DAΦNE - Frascati, Nov.16-19,1999 Frascati Physics Series Vol.XVI (2000); . J.A. Oller, hep-ph/0007349 (2000).
- [5] A. Bramon et al., Phys. Lett. B 494 (2000), 221; R. Escribano, hep-ph/0012050; A. Bramon et al., hep-ph/0105179 (to be published in Phys. Lett. B).
- [6] D. Black et al., Phys. Rev. D61 (2000), 074001.
- [7] F. Close, N. Isgur and S. Kumano, Nucl. Phys. B389 (1993) 513; See also N. Brown, F.E. Close in: L. Maiani, G. Pancheri, N. Paver (Eds.), The Second Dafne Handbook, INFN-LNF, 1995, p.649.
- [8] R. L. Jaffe, Phys. Rev. D15 (1977) 267; M. Alford, R.L. Jaffe, Nucl. Phys. B578 (2000) 367.
- [9] J. Weinstein and N. Isgur, Phys. Rev. Lett. 48 (1982) 659
- [10] N.A. Törnqvist, Z. Phys. C68 (1995) 647 and references therein.
- [11] F.E. Close, A. Kirk, hep-ph/0106108 (2001).
- [12] M. Adinolfi et al.[The KLOE Collaboration], LNF-01/017 (P) (2001), submitted to Nucl. Intr. and Meth.
- [13] M.N.Achasov et al., Phys. Lett. B485 (2000), 349.
- [14] M.N.Achasov et al., Phys. Lett. B479 (2000), 53.
- [15] M.N.Achasov et al., Nucl. Phys. B569 (2000), 158.
- [16] D.E.Groom et al., The European Physical Journal C15 (2000), 1.
- [17] R.R. Akhmetshin et al., Phys. Lett. B462 (1999), 280.
- [18] The KLOE Collaboration, hep-ex/0006036.
- [19] N.N. Achasov and V.V. Gubin, Phys. Rev. D63 (2001) 094007.
- [20] M.N. Achasov et al., JETP Lett. 72 (2000), 282; R.R. Akhmetshin et al., Phys. Lett. B509 (2001), 217.